3. ALIGNMENT OF FULLERENES FOR QUANTUM COMPUTATION

The physical realization of a quantum computer (QC) is a very challenging task for which solving nowadays there are lots of different proposals. The most promising implementations seem to be those which are based on solid state devices since they are supposed to show good scalability. In this chapter a possible QC architecture based on group V endohedral fullerenes will be described. A key step is the creation of an aligned linear chain of fullerenes on a solid surface which can be realized for example with scanning tunneling microscope. Since the detection of single electron spin (although performed in some cases) remains still a big challenge, experiments with ensemble of fullerenes are done in this work.

3.1 Fullerene Based Quantum Computer

In this section we present the concept of a quantum computer based on the group V endohedral fullerenes, which was developed by W. Harneit in 2002 [17]. A scheme of the device is shown in Fig. 3.1. As already mentioned in the introduction, quantum

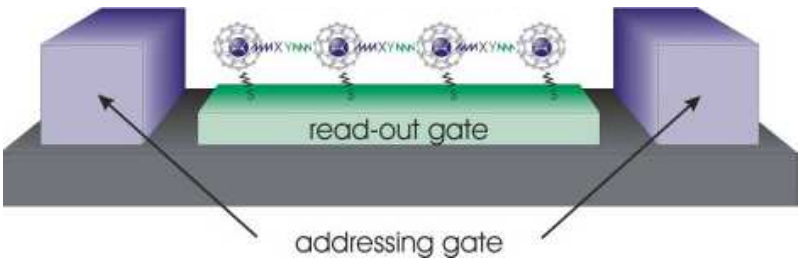

Fig. 3.1: Graphical visualization of the solid state spin quantum computer based on endohedral fullerenes.

computers could have great advantages over the classical ones. The main problem is the scalability, namely coupling several hundreds of qubits to each other and controlling each of them separately. This obstacle could be overcome in a solid state approach, for example using phosphorus donors in silicon as proposed by Kane [69], but even with today's technology it is still a very big challenge. Another possible concept is the quantum cellular automaton (QCA), where linear chains of three

alternating qubit types A-B-C [70] or even two A-B [71, 72] are used but no control over individual spins is required.

Electron spins are more promising qubits than nuclear spins, because the time to manipulate the former is about thousand times shorter than for the latter. A typical MW pulse is about 10-100 ns, while RF pulses in NMR are usually in the order of micro- or milliseconds. However it is very difficult to isolate an electron spin from its environment and the usual relaxation times are few microseconds in the best cases. The endohedral atom in $N@C_{60}$ and $P@C_{60}$ is very well shielded from the surrounding which leads to the unusually long relaxation times for molecules - T_1 is about a second at $T = 5$ K [47] and T_2 reaches 400 μs in diluted samples (see next chapter). Thus they are very good candidates for qubits in a QCA [17]. The fullerenes in Fig. 3.1 are aligned in a linear A-B chain on a solid state surface where A is for example $N@C_{60}$ and B is $P@C_{60}$. Each of them could be chemically bonded to the surface and/or to the neighboring fullerenes, the most important thing being that the distance between the qubits is well defined. The addressing gate consists of a pair of micron sized wires placed on both sides of the fullerene string. When varying the magnitude of the current, a controlled magnetic field gradient across the fullerene chain can be applied. Thus each endohedral atom has a different resonance frequency and can be addressed selectively using MW pulses. Such pulses are also used ro realize quantum gates and some of the necessary sequences have already been calculated [19, 18].

The biggest obstacle for this experimental quantum computing approach (and other solid-state proposals based on spin-qubits) is the read out of the information stored in the qubits. The problem is that a single spin read-out is needed while in most of the quantum mechanical experiments an ensemble of particles is measured. A single spin read-out of electron spins was recently demonstrated for nitrogen-vacancy (NV) center in diamond using optically detected magnetic resonance (ODMR) [73] at room temperature. The ground state of the NV center is triplet as is the first excited state, and the allowed transition between them has a strong fluorescence. The intensity of the latter depends on the electron spin quantum state and this is used for the ODMR detection of a single NV defect center [73] and to measure coherent oscillations in it [74] at room temperature. It might be possible to couple an NV center to each endohedral fullerene so that the spin information can be transferred to the center and read out via ODMR.

Although single spin read out of endohedral fullerenes is not possible at present, alignment of them in a matrix is expected to lift the degeneracy of the electron spin $S = 3/2$ system. Relaxation QC experiments with these order structures provides helpful information about their properties (see later chapters).

3.2 Alignment of Endohedral Fullerenes in Liquid Crystal

The first attempt to orient endohedral fullerenes was to dissolve them in different liquid crystals (LC) [75, 76, 77] and a certain alignment was expected when the sample is placed in a magnetic field. The ESR spectrum of $N@C_{60}$ in 4-methoxybenzylidene-4-n-butylaniline (MBBA) is shown in Fig. 3.2. The achieved orientation was not very

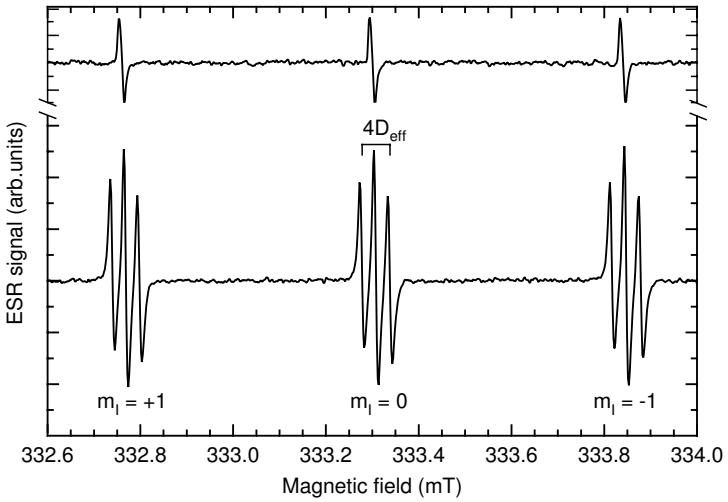

Fig. 3.2: ESR spectrum of $N@C_{60}$ in solution (above) and $N@C_{60}$ in the liquid crystal 4-methoxybenzylidene-4-n-butylaniline (MBBA) [75]. The ZFS D_{eff} is 0.09 MHz (see table 3.1)

good, but the results are still encouraging as the degeneracy in the spin $S = 3/2$ was partially lifted suggesting that there is some orientation of the fullerenes. The ESR spectra show that every $N@C_{60}$ line is split into three components. This suggests that the symmetry of the fullerene carbon cage is lowered and from the spectra $D = 0.09$ MHz is obtained. $N@C_{70}$ in LC shows larger D as it is expected since C_{70} carbon cage has lower than C_{60}. Surprisingly, $N@C_{60}$-C_{60} mixture with LC does not increase the ZFS of the endohedral atom, although the symmetry of this molecule is significantly lower. In all cases no change or anisotropy of the hyperfine constant is observed. The relaxation of the endohedral atom was not significantly affected, for $N@C_{60}$ the FWHH is about 120 kHz and for $N@C_{70}$ 170 kHz [75]. The corresponding ZFS parameters are summarized in table 3.1.

endohedral	host matrix	D (MHz)
$N@C_{60}$	polycrystalline C_{60} solid, $T < 260$ K	0.52
$N@C_{60}$	MBBA	0.09
$N@C_{70}$	MBBA	0.418
$N@C_{60}(COOC_2H_5)_2$	powder	6.02
$N@C_{60}$-C_{60}	powder	13.44
$N@C_{60}$-C_{60}	MBBA	0.18

Tab. 3.1: Comparison of the ZFS of $N@C_{60}$, chemically modified $N@C_{60}$, $N@C_{70}$ and $N@C_{60}$-C_{60}. [47, 75, 77].

3.3 Alignment of Endohedral Fullerenes in a Solid State Matrix

The orientation of $N@C_{60}$ in LC has some significant practical shortcomings, namely the ZFS was too small to be used for selective transition excitation and it can be use in principled only at room temperature or down to the freezing point of the LC. Alternative approach is to build a crystal (or any other structure) with the fullerenes themselves, the only obstacle being their limited thermal stability [63].
The inclusion of "empty" fullerenes C_{60} and C_{70} as guests in the solid state matrix of 2,4,6-tris-(4-bromophenoxy)-1,3,5-triazine (BrPOT) (Fig. 3.3) was first reported by H. Süss in the Hulliger group at the University of Berne [78]. The obtained structure is a hexagonal crystal with one-dimensional parallel channels whose cross sectional view is shown in Fig. 3.4. X-Ray diffraction (XRD) measurements reveal diffuse

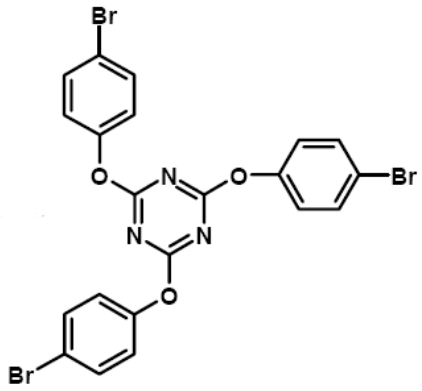

Fig. 3.3: The chemical formula of 2,4,6-tris-(4-bromophenoxy)-1,3,5-triazine (BrPOT).

electron density for the encapsulated fullerenes, indicative of a liquid- or glass-like phase for the fullerene guests. Moreover, there are three solvent molecules (toluene or CS_2) per C_{60} in the channels so it seems that solvent inclusion is important for the building of the crystal. Indeed, thermogravimetric measurements revealed a loss of toluene from the guest-host system first at 200 °C and decomposition of the

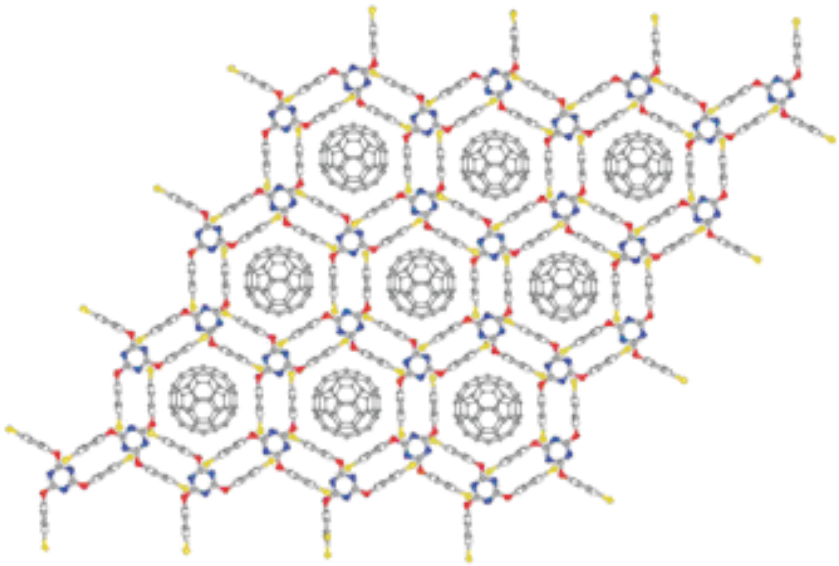

Fig. 3.4: A cross sectional view of the idealized (no solvent inclusion and the fullerenes are located) hexagonal crystal modification of the C_{60} inclusion in BrPOT [78].

crystal at 300-380 °C. In a toluene-BrPOT inclusion structure without fullerenes, the solvent escapes already at 70 °C.

The inclusion of group V endohedral fullerenes was first performed in collaboration with the Hulliger group as described in [78] and subsequently continued in our group. BrPOT and fullerenes were dissolved together in CS_2 or toluene. Afterwards the solution was heated to just below its boiling point and then cooled down very slowly (about 1°C per hour) to room temperature. Two different crystal types were obtained in every run - the hexagonal one as expected from [78] and a new rhombohedral structure shown in Fig. 3.5 [79]. Unlike in the hexagonal crystals, there are no channels in the rhombohedral modification. Each fullerene is trapped in an individual cell made of several BrPOT molecules as can be seen in Fig.3.5c and there are no enclosed solvent molecules. The C_{60} and the BrPOT molecules are fully oriented, even the different length of the 6-6 and 5-6 carbon bonds in the fullerene cage could be measured in good agreement with the literature. The full crystal structure is available from the Cambridge Crystallographic Data Centre (CCDC) at http://www.ccdc.cam.ac.uk/data_request/cif under record number CCDC-297690. $N@C_{70}$ and BrPOT build only hexagonal crystals. Again only the BrPOT channels could be resolved in XRD experiments. All crystallographic data are summarized in table 3.2 and photos of the two crystal types are shown in Fig. 3.3. Fullerenes and BrPOT crystallized from CS_2 show only the hexagonal crystal structure and the lattice parameters are very similar to those of the crystals obtained from toluene solution, as reported in table 3.2.

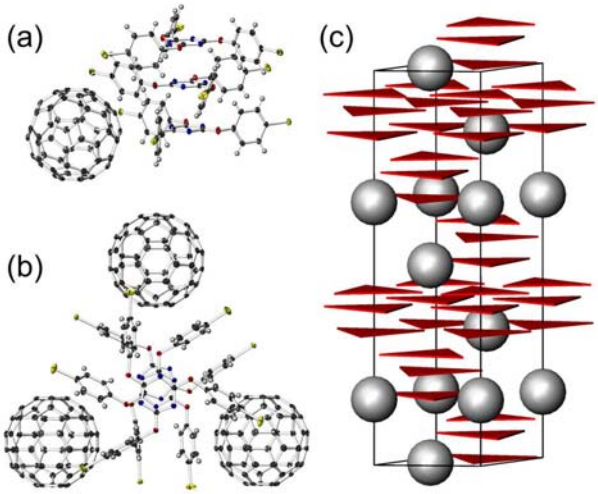

Fig. 3.5: Rhombohedral crystal modification of the C_{60} inclusion in BrPOT, (a) the simplest building block of the crystal consisting of one C_{60} and three BrPOT molecules. (b) The same block rotated at 90° with three neighboring C_{60} molecules. (c) Unit cell of the rhombohedral crystal. C_{60} molecules are drawn as balls and BrPOT molecules as triangles whose apices are the Br atoms.

crystal system	hexagonal	rhombohedral
space group	$P6_3/m$	R3c
unit cell $\alpha=\beta=90°$, $\gamma=120°$	$a = b = 15.811$, $c = 6.8634$ Å	$a = b = 16.022$, $c = 59.487$ Å
BrPOT per unit cell	2	18
BrPOT per C_{60}	~ 5	3
C_7H_8 per C_{60}	~ 3	0

Tab. 3.2: Crystallographic data for the two structures of C_{60} in BrPOT crystallized from toluene.

The co-crystallization of the N@C_{60}-C_{60} and BrPOT from CS_2 showed also only hexagonal crystals, but unfortunately the ESR signal was too weak for detection.

3.3.1 ESR Measurements

In all inclusion structures measured in this work no change or anisotropy of the hyperfine fine constant a and of the g-factor was detected. The ESR spectrum of the hexagonal crystals of N@C_{60} in BrPOT obtained from toluene solution is very similar to the spectrum of solid N@C_{60} (Fig. 3.7) [80]. The only difference is that the lines are inhomogeneously broadened with FWHH = 2.8 MHz, so it is possible that they cover a fine structure, while for N@C_{60} in solid state the FWHH is 450 kHz [46]. The increased line width can be explained by the presence of protons in the BrPOT matrix and in the toluene molecules included in the channels. The crystals obtained

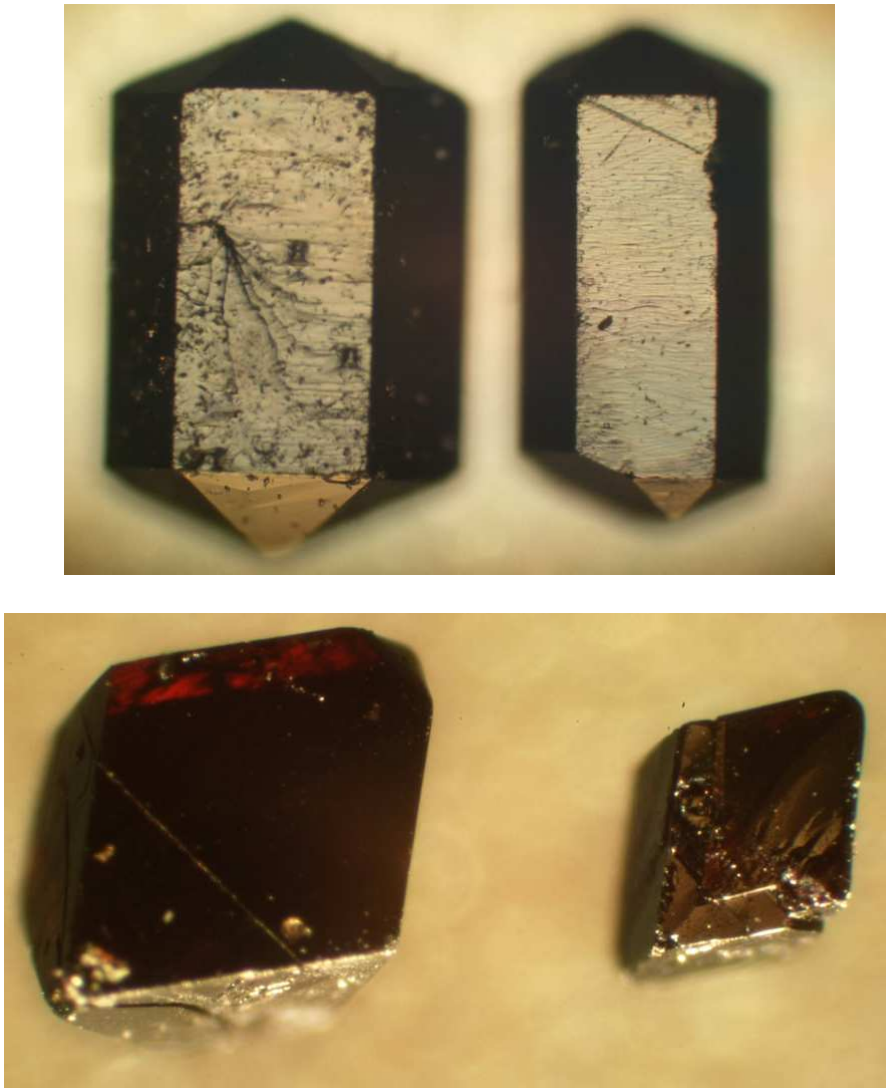

Fig. 3.6: Photos of the hexagonal (top) and rhombohedral (bottom) crystal modifications of C_{60} in BrPOT crystallized from toluene solution.

from CS_2 solution are hexagonal and a fine structure is observed ($D = 0.9$ MHz). The lines are less broad (FWHH = 2 MHz) than in the toluene samples as can be seen in Fig. 3.7. The measured line width is about 20 % smaller when compared to

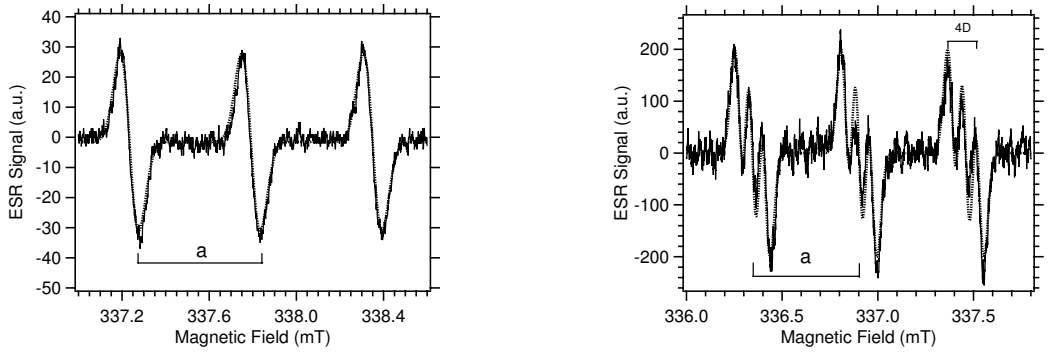

Fig. 3.7: ESR spectrum of single hexagonal crystals of N@C_{60} in BrPOT, crystallized from toluene (left) and CS_2 solution (right). The dotted lines are simulations.

the toluene crystals confirming that the toluene inclusion contributes to the width of the ESR line. The ESR spectra of P@C_{60} hexagonal crystals (both from toluene and CS_2) also do not show any ZFS (Fig. 3.8) and only strong line broadening is observed (see table 3.3). This result is quite surprising since the phosphorus atom should be much more sensitive to deformation of the fullerenes carbon cage than the nitrogen atom, if the increase of the hyperfine constants with respect to the free atoms is taken into account (see table 2.1). The line widths of P@C_{60} in hexagonal BrPOT is larger for the crystals obtained from CS_2 than from toluene solution in contrast to N@C_{60}. Possibly there is some non-vanishing ZFS that broadens the lines, but it cannot be resolved in the spectrum.

N@C_{70} and BrPOT build only hexagonal crystals from both toluene and CS_2 solutions. A larger ZFS is expected as the symmetry of the C_{70} cage (D_{5h}) is lower than the cage symmetry of C_{60} (I_h). A similar effect was already observed in LC solutions (cf. table 3.2). At room temperature, no fine structure is detected in the ESR spectrum as shown in Fig. 3.9, while at $T = 100$ K a ZFS of $D = 2.16$ MHz could be detected. These results suggest that rotational and/or translational movement of C_{70} is still possible at room temperature, averaging the ZFS to a value lower than the measured line width. At $T = 100$ K the movement is hindered at the timescale of ESR, i.e. N@C_{70} molecules assume fixed positions in the channels. This can be compared to muon-spin-rotation experiments of solid C_{70} [81], which reveal that below $T = 150$ K their position is fixed.

N@C_{60} and P@C_{60} in single rhombohedral crystals always exhibit significant ZFS as shown in Fig. 3.10 and Fig. 3.12. In order to describe the electron spin properties of the endohedral atom the ZFS term 1.14 should be added to the Hamiltonian 2.1

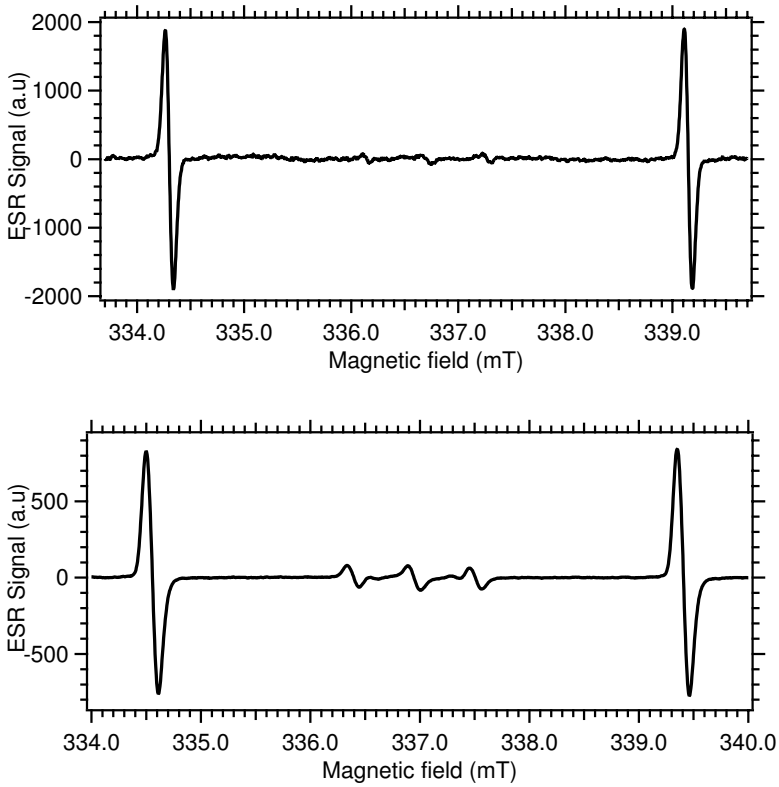

Fig. 3.8: ESR spectrum of single hexagonal crystals of $P@C_{60}$ in BrPOT crystallized from toluene (top) and CS_2 solution (bottom). Three lines in the middle are from $N@C_{60}$ contaminations in the $P@C_{60}$ sample.

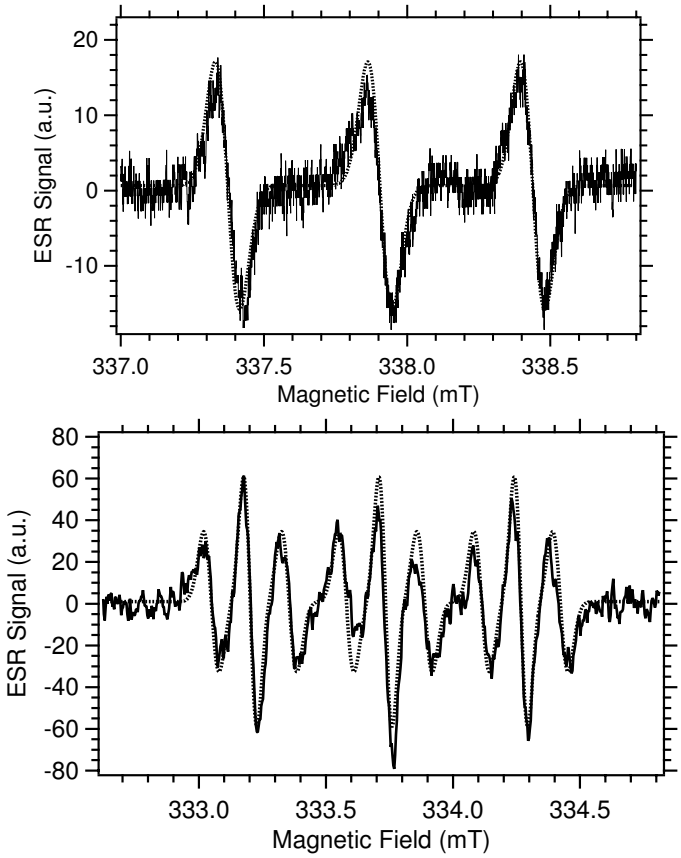

Fig. 3.9: ESR spectrum of single hexagonal crystals $N@C_{70}$ in BrPOT crystallized from toluene measured at room temperature (top) and at $T = 100$ K. Dotted lines are simulations with parameters reported in table 3.3.

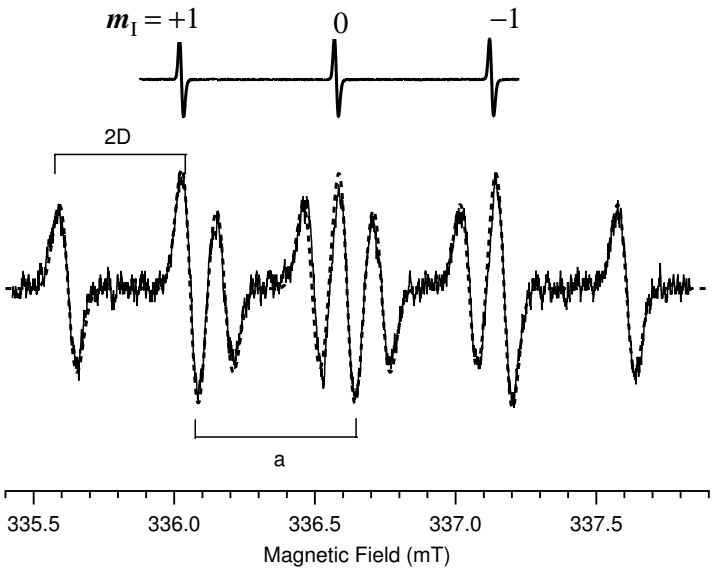

Fig. 3.10: ESR spectrum of a single crystal of N@C_{60} in rhombohedral BrPOT (bottom) and of a polycrystalline N@C_{60} (above). The orientation angle is $\theta = 20°$ and $D = 8.1$ MHz (2.89 G) (see text). The dotted line is a simulation with the above parameters.

and the calculated energy levels are (see section 1.4.2):

$$E_{m_S,m_I} = m_S\hbar\omega_0 + m_I m_S\hbar a + (m_S^2 - \frac{5}{4})\hbar D(\theta) + m_I\hbar\omega_I \tag{3.1}$$

and the resonant field of each line according to equations (1.16-3) is:

$$B_{m_S \to m_{S-1}} = B_0 - a m_I - \frac{D(\theta)}{g\mu_B}(2m_S - 1) \tag{3.2}$$

where $D(\theta) = D_0(3\cos^2\theta - 1)$ and $m_S = -\frac{3}{2}, -\frac{1}{2}, +\frac{1}{2}, +\frac{3}{2}$, $m_I = +\frac{1}{2}, -\frac{1}{2}$ for P@C_{60} and $m_I = -1, 0, +1$ for N@C_{60}, $B_0 = \frac{\hbar\omega_0}{g\mu_B}$, D_0 is the ZFS parameter (see section 1.4.2) and θ is angle between the applied magnetic field and the crystal symmetry axis.

As in the case of the hexagonal crystals, no anisotropy of g or a could be detected and they have the same values as for the "free" endohedral fullerenes (within experimental error). The spectrum in Fig. 3.10 shows clearly that each of the three hyperfine lines of N@C_{60} is split into three lines according to equation (3.2). The lines corresponding to transition $m_S = +1/2 \leftrightarrow m_S = -1/2$ can be easily distinguished from the ones with transitions $m_S = -1/2 \leftrightarrow m_S = -3/2$ ($m_S = +3/2 \leftrightarrow +1/2$) as the former do not depend on the angle θ and have larger intensity than the latter. The

ratio of their intensities expected from theory [82]is:

$$I_{+1/2;-1/2} : I_{+3/2;1/2} = |\langle +1/2|S_-|-1/2\rangle|^2 : |\langle +3/2|S_-|+1/2\rangle|^2 = 4:3$$

where $S_- = S_x - iS_y$ is the lowering spin operator. The experimentally measured ratio is in good agreement with this value. The presence of ZFS indicates a certain deformation of the fullerene carbon cage and a lowering of its symmetry. Each line is much broader (FWHH = 2 MHz) than that of bulk N@C_{60} (FWHH = 450 kHz [46]), as in the hexagonal crystals, again the possible reason being the protons of the BrPOT matrix. The angular dependent transitions are about 10 % broader, which can be explained by a Gaussian distribution δD of the ZFS parameter D as confirmed by simulations using the EasySpin package [60]. In Fig. 3.11 the position of each line in the spectrum is plotted as a function of the angle θ together with simulations accordingly to equation (3.2). The fine structure disappears at the magic

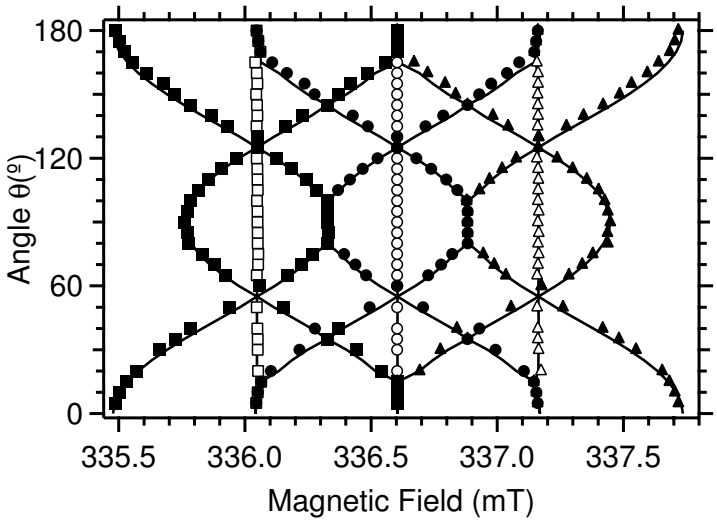

Fig. 3.11: Position of the ESR lines of N@C_{60} in rhombohedral BrPOT. Filled (empty) markers correspond to transitions with $m_S = 3/2 \leftrightarrow 1/2$ and $m_S = -1/2 \leftrightarrow -3/2$ ($m_S = +1/2 \leftrightarrow -1/2$). Squares, circles and triangles indicate respectively $m_I = +1$, $m_I = 0$ and $m_I = -1$. The solid curves are simulations.

angle $\theta = 54.7°$ when each group of three lines collapse into one. All parameters are summarized in table 3.3.

The hyperfine constant of P@C_{60} is about ten times larger than that of N@C_{60} (table 2.1) which suggests that the electron spin of the phosphorus atom is more sensitive to the deformations of the fullerene cage. This is confirmed by the larger ZFS of P@C_{60} in the rhombohedral crystal modification, which can be seen in the ESR spectra of a single crystal shown in Fig. 3.12. Similar to the encapsulated N@C_{60}, the lines with transition $m_S = +1/2 \leftrightarrow -1/2$ are narrower and have more

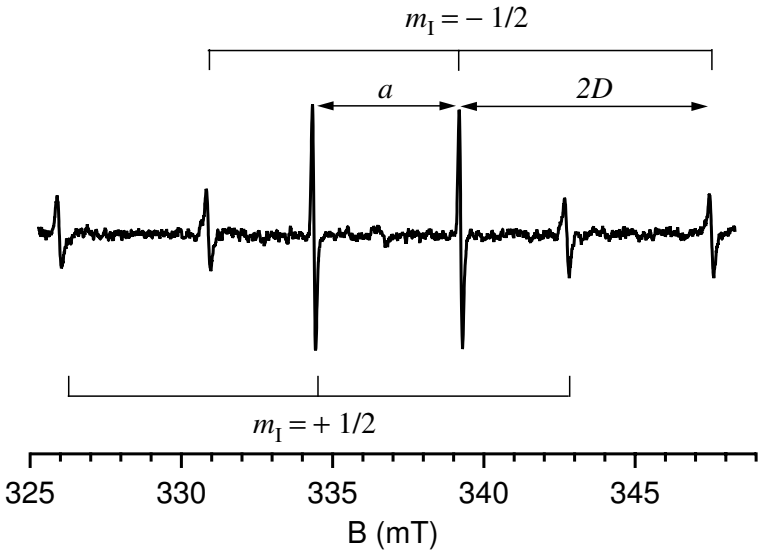

Fig. 3.12: ESR spectrum of a single rhombohedral crystal P@C_{60} in BrPOT. The sample is oriented at angle $\theta = 0$ where the ZFS is maximal.

intensity than the lines with transitions $m_S = -1/2 \leftrightarrow -3/2$ ($m_S = +3/2 \leftrightarrow +1/2$) and again the former do not depend on θ. The resonance fields of each transition for different angle θ are plotted in Fig. 3.13 together with simulations. From this data and from the simulation a ZFS $D = 127$ MHz is extracted. It is noteworthy that the fullerene carbon cage is deformed although it is not chemically bonded to the crystal matrix and that this effect can be seen when using the endohedral atoms as a probe inside the crystal. The distortion of endohedrals dissolved in liquid crystal fullerenes, although much smaller than in BrPOT, is also not caused by chemical modification.

The temperature dependence of the ZFS of P@C_{60} in rhombohedral BrPOT is

endohedral	solvent	crystal type	D (MHz)	δD (MHz)	FWHH (MHz)
N@C_{60}	toluene	hexagonal	0	-	2.8
		rhombohedral	8.01	0.35	2
	CS_2	hexagonal	0.945	0.1	1.8
N@C_{70}	toluene	hexagonal	0	-	2.8
	toluene[a]	hexagonal	2.16	0.5	1.8
P@C_{60}	toluene	hexagonal	0	-	2.3
		rhombohedral	127	1.7	4.8
	CS_2	hexagonal	0	-	3.06

[a] Measured at T = 100K

Tab. 3.3: ZFS parameters and ESR lines widths for different group V endohedral fullerenes in the two BrPOT crystal structures.

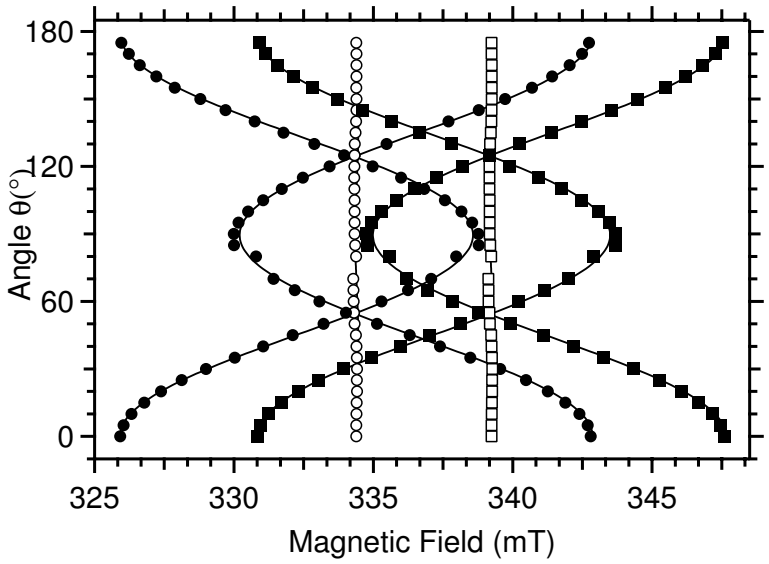

Fig. 3.13: Position of the ESR lines of P@C_{60} in rhombohedral BrPOT as a function of θ. Filled (empty markers) correspond to transitions with $m_S = 3/2 \leftrightarrow 1/2$ ($m_S = +1/2 \leftrightarrow -1/2$). Circles (squares) indicate $m_I = -1/2$ ($m_I = +1/2$). The solid curves are simulations.

shown in Fig. 3.14. A continuous increase in the size of the fine structure D is observed when raising the temperature from $T = 10$ K to $T = 210$ K, where a step-like increase is seen. Above 210 K, and up to room temperature, D grows again continuously. This is ascribed to a phase transition in the crystal structure, as this ESR parameter is very sensitive to the environment of the endohedral atom. A slight increase of the hyperfine constant a is also observed (Fig. 3.15 as the temperature increases, like in bulk N@C_{60} (P@C_{60}) but the step-like behavior at $T = 210$ K is not seen. It is likely that the phase transition does not involve a significant change in the lattice parameters (i.e. additional "squeezing" of the fullerene cage). Rather, a reorientation of the C_{60}molecules is likely to occur. The phase transition was not detected in XRD, since only measurement at $T = 100$ K were preformed.

In order to determine whether the sign of D is positive or negative, an ESR measurement should be done at lower temperature and possibly at higher MW frequency. The level spacing increases at higher magnetic fields and/or lower temperatures and the lowest levels are increasingly populated. Since the ESR signal is proportional to the population difference lines corresponding to the transition $m_S = -1/2 \leftrightarrow m_S = -3/2$ are expected to have more intensity than the transition $m_S = +1/2 \leftrightarrow m_S = +3/2$ if the ZFS D is positive. The echo detected spectrum of P@C_{60} in BrPOT at $T = 10$ K in W-band (94 GHz, $B_0 = 3.35$ T) is shown in Fig. 3.16. The intensity of the two low field lines is clearly decreased compared to

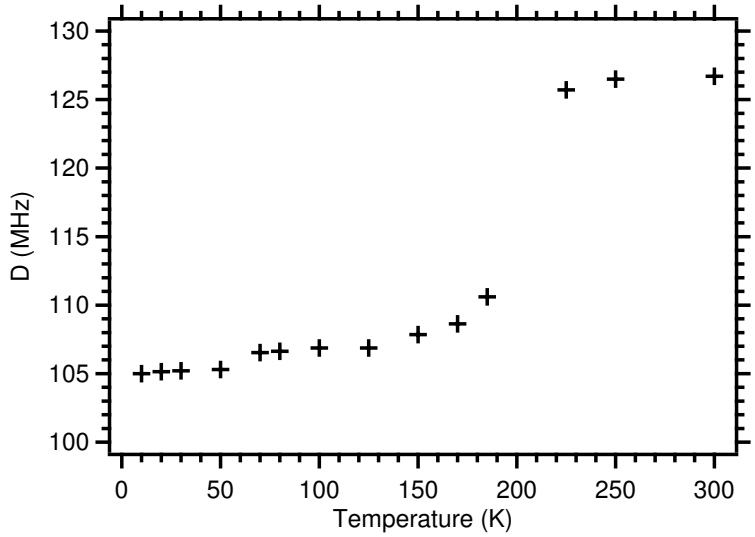

Fig. 3.14: Temperature dependence of the ZFS of P@C_{60} in BrPOT measured in W-Band (MW frequency 94 GHz). The sudden change of D at $T = 210$ K is possibly due to a phase transition in the crystal structure.

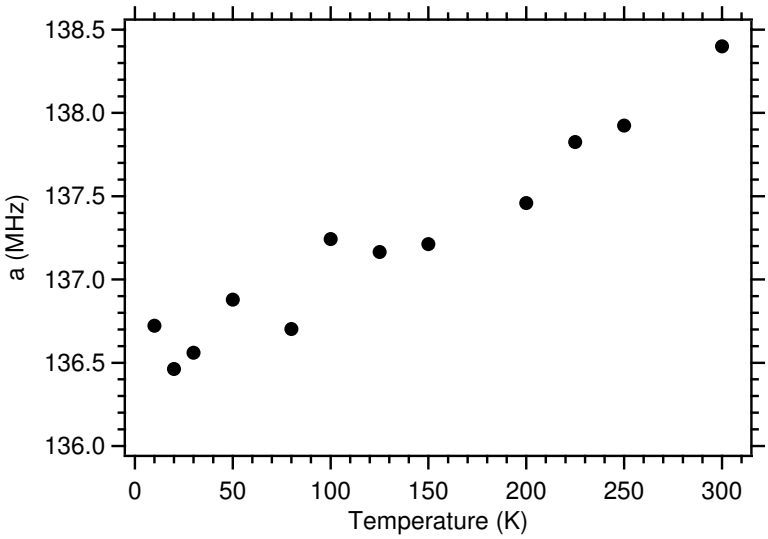

Fig. 3.15: Temperature dependence of the hyperfine constant a of P@C_{60} in BrPOT measured in W-Band.

the two high field lines, so D must be positive.

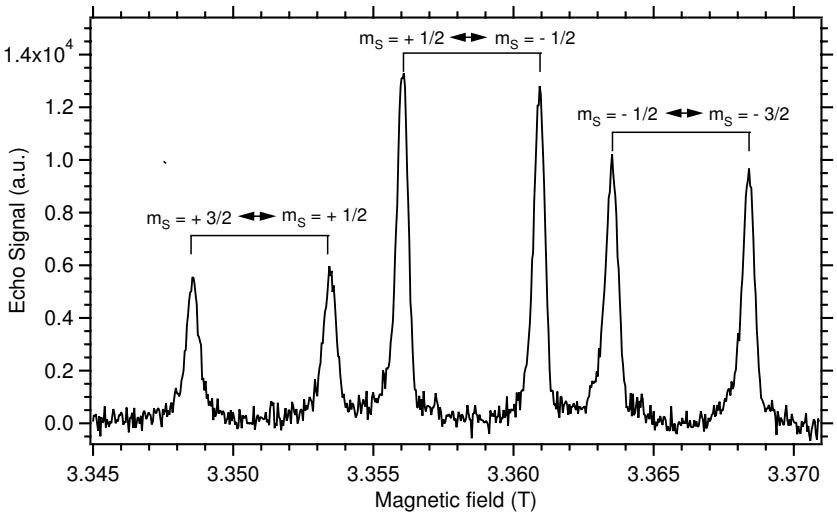

Fig. 3.16: Echo detected spectrum of P@C_{60} in BrPOT at $T = 10$ K and orientation angle $\theta = 0$. The transitions $m_S = -1/2 \leftrightarrow m_S = -3/2$ have larger intensity than the $m_S = -1/2 \leftrightarrow m_S = -3/2$ transitions.

3.3.2 ENDOR Measurements

The ENDOR frequencies of P@C_{60} in BrPOT in W-Band can be calculated using equation (1.48). The Larmor frequency in MHz of the phosphorus nucleus at that field is:

$$\nu_L = \frac{\gamma_P B_0}{2\pi} = \frac{1.08394 \times 10^8 \times 3.35}{2\pi} = 57.8$$

and the four frequencies (again in MHz) are:

$$\nu_1 = 127 \quad \nu_2 = 10.8$$
$$\nu_3 = 148 \quad \nu_4 = 263.6$$

Mims ENDOR spectra (see chapter 1.6) are shown in Fig. 3.17. The line at 263.6 MHz could not be detected, because the resonator which was used for the experiment is specified for RF frequencies up to 200 MHz. Its frequency bandwidth also limits the detection of the line at 10 MHz which can barely be measured (not shown in the figure). All ENDOR lines are broadened (FWHH $\approx$ 22 kHz) by the presence of hydrogen atoms in the BrPOT matrix. Nevertheless, the good separation of the ESR lines allows to pulse selectively on each ESR transition and to identify which ENDOR transitions connect which energy levels. This is very important for the

preparation of pure states and entanglement which will be discussed later in detail (see chapter 5).

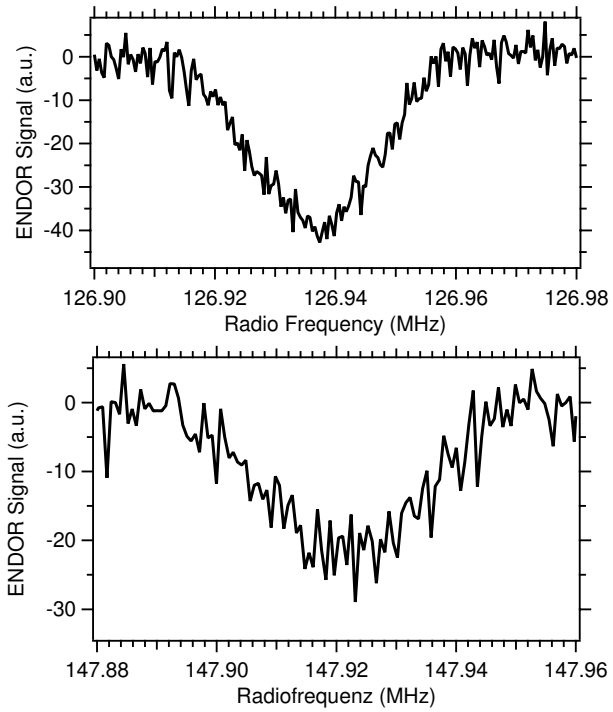

Fig. 3.17: Two of the four ENDOR lines of P@C_{60} in BrPOT - $\nu_1 = 127MHz$ (top) and $\nu_3 = 148$ MHz (bottom).

3.3.3 Distant ENDOR

The increased line width of P@C_{60} in BrPOT can be ascribed to the presence of protons in the BrPOT matrix. In order to prove this conjecture, the coupling between the electron spins of the endohedral atom and the neighboring protons can be measured with the help of distant ENDOR. For these experiment the Mims ENDOR pulse sequence was used and the RF pulse was swept about the Larmor frequency of the neighboring nuclear spins. This method was first used by Lambe *et.al*, to study the coupling of an electron spin (Cr^{3+}) to distant ^{27}Al nuclei in ruby [83]. In the literature these type of experiments are divided in two types - distant ENDOR and matrix ENDOR [84]. The former considers strong hyperfine coupling between a paramagnetic center in a crystal with the neighboring nuclear spins [83, 85], while the latter is usually used for magnetic dipolar electron-nuclear spin interaction in amorphous or polycrystalline materials [86, 87].

In this work coupling between the endohedral phosphorus atom and all the neighboring nuclear spins was investigated, namely protons ^{1}H (I = 1/2), ^{13}C (I = 1/2),

^{79}Br and ^{81}Br. The latter two have very similar Larmor frequencies. The successful detection depends on the natural abundance and the γ of the corresponding nuclear spin. A clear ENDOR signal was only detected at the Larmor frequency of ^{1}H and the spectrum is shown in Fig. 3.18. The presence of this strong signal

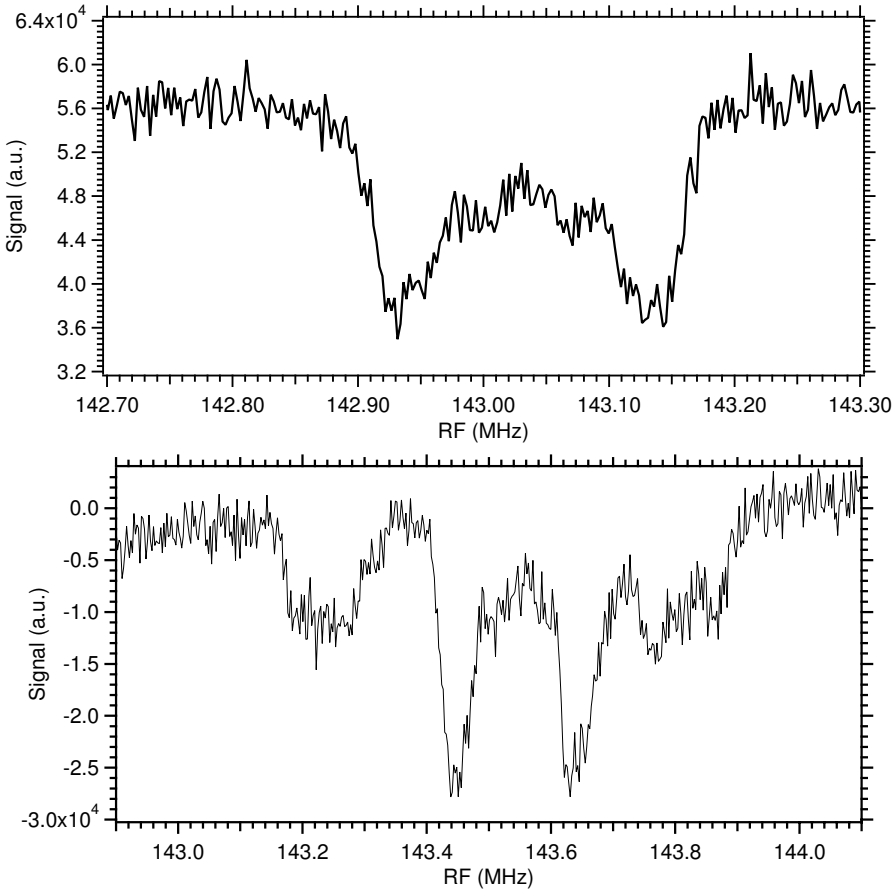

Fig. 3.18: Distant ^{1}H-ENDOR of P@C_{60} in BrPOT. The detection is on ESR transition with $m_S = +1/2 \leftrightarrow m_S = -1/2$ (top) and with $m_S = -1/2 \leftrightarrow m_S = -3/2$ (bottom).

(compared to the usual or local ENDOR signal) proves that the ESR lines are really inhomogeneously broadened by the protons in BrPOT matrix. As there is little transfer of spin density from the endohedral phosphorus atom to the carbon cage [57], the ENDOR signal can be considered as matrix ENDOR. The Hamiltonian of the magnetic dipolar interaction between an electron spin and many protons, which are approximated as point-like dipoles, is given by the expression:

$$H_{DD} = \mu_0 \hbar g_E \mu_B \gamma_H \sum_{i=1}^{N} \frac{(3\cos^2(\theta_i) - 1)}{r_i^3} I_z^i S_z \tag{3.3}$$

where r_i is the distance between proton i and the electron, while θ_i is the angle between $\vec{r}$ and the applied magnetic field $\vec{B_0}$. I_z^i and S_z are the z spin operators of proton i and the electron spin.
Assuming that there are many protons with the same M_I, the Hamiltonian 3.3 can be simplified to:

$$H_{DD} = \frac{\mu_0 \hbar g_E \mu_B \gamma_H}{2\bar{r}^3} S_z I_z = \frac{B}{\bar{r}^3} S_z I_z \tag{3.4}$$

where $(3\overline{\cos^2(\theta_i)} - 1) = 1/2$ was used and $\bar{r}$ is the mean electron-proton distance. With the simplified Hamiltonian 3.4 the energy levels of the this system are:

$$E(m_S, m_I) = m_I \hbar \omega_p + m_S m_I \frac{B}{\bar{r}^3} \tag{3.5}$$

where $m_I \hbar \omega_p$ is the proton Zeeman energy with ω_p the proton Larmor frequency. Using the NMR selection rules $\Delta m_I = \pm 1$ then four lines are expected in the ENDOR spectrum. For the two transitions $(+1/2, m_I) \leftrightarrow (+1/2, m_I - 1)$ and $(-1/2, m_I) \leftrightarrow (-1/2, m_I - 1)$ the spectral lines are shifted from ω_0^p at $B/2\bar{r}^3$ and $-B/2\bar{r}^3$ respectively. For the other two transitions $(+3/2, m_I) \leftrightarrow (+3/2, m_I - 1)$ and $(-3/2, m_I) \leftrightarrow (-3/2, m_I - 1)$ the shifts are correspondingly $3B/2\bar{r}^3$ and $-3B/2\bar{r}^3$. The separation of the former two transitions is expected to be $B/\bar{r}^3$, while the separation of the latter two is $3B/\bar{r}^3$.
Detection on the $(+1/2, -1/2)$ ESR transition yielded two lines in the H-ENDOR spectrum as shown in Fig. 3.18(top). Detection on the $m_S = -1/2 \leftrightarrow m_S = -3/2$ ESR transition gives rise to 4 lines (Fig. 3.18(bottom)) with a ratio of the inner line separation to the outer one of $1 : 3$, as expected from the calculations above. One can thus extract $B/\bar{r}^3 = 200 \pm 2$ kHz from the spectra which corresponds to a mean distance $\bar{r} = 5.85\mathring{A}$ between the endohedral electron spin and the protons. The XRD measurements reveal larger values for r_i and $\bar{r}$ (about $6.7\mathring{A}$). The latter experiments were performed at temperature $T = 100$ K, while the H-ENDOR was measured at $T = 50$ K, but this temperature difference can not still explain the descrepancies between the two experiments. Another possibility would be that the point-like dipole for the electron spin is not adequate enough model since the latter are p electrons. Moreover, the pulse sequence for the H-ENDOR measurements were not additionally optimized. The time τ between the first two pulses of the Mims sequence should be varied together with the power of the RF pulse. Otherwise so-called blind spots appear in the ENDOR spectrum, and (or) the line is broadened by the RF power [87, 88].

3.4 Conclusions

It was found that the group V endohedral fullerenes can be encapsulated as guests in the host matrix of BrPOT. Thus guest-host structure builds two crystal types - hexagonal and rhombohedral. The former is obtained from both toluene and CS_2 solution while the latter crystallizes only from toluene. The hexagonal crystals consists of parallel channels built from the BrPOT molecules in which the fullerenes are situated together with solvent molecules. XRD measurements reveal diffuse density for the guests similar to glass like phase. In the rhombohedral structures there is an individual "pocket" from BrPOT molecules for each fullerene where there are no channels and no solvent inclusions.

The ESR spectra of the hexagonal crystal modification of $N@C_{60}$, $N@C_{70}$ and $P@C_{60}$ inclusion in BrPOT from toluene solution show inhomogeneously broadened lines. The gyromagnetic factor g and the hyperfine constant are isotropic and remain unchanged compared to the values of the bulk endohedrals. No ZFS is detected at room temperature, while $N@C_{70}$ crystals show fine structure ($D = 2.16$ MHz) at $T = 100$ K. When the co-crystallization is performed from CS_2 solution only hexagonal crystals are obtained with smaller line broadening compared to the toluene crystals (see table 3.3) where ZFS was detected only for $N@C_{60}$ in BrPOT.

In the new rhombohedral crystals both $N@C_{60}$ and $P@C_{60}$ in BrPOT show significant fine structure with $D = 8.01$ MHz and $D = 127$ MHz respectively. The temperature dependence of ZFS show jump of its value at $T = 210$ K suggesting a phase transition in the crystal. Low temperature ESR spectra at W-band shown increase of the lines from transition $m_s = -1/2 \leftrightarrow m_s - 3/2$ hence a positive sign for the ZFS parameter D is deduced.

Proton distant ENDOR measurements reveal coupling of the endohedral atom to the neighboring protons ion the BrPOT matrix, a process which explains the strong broadening of the ESR spectral lines.

The orientation dependence of the lines from transitions involving states with $|m_s| = 3/2$ allow transition selective pulsing which provides additional information about the spin structure (see next chapters).